Grime, J. K. (1985) in *Analytical Solution Calorimetry* (Grime, J. K., Ed.) pp 299-390, Wiley & Sons, New York.
Harris, D. C., & Aisen, P. (1989) in *Iron Carriers and Iron Proteins* (Loehr, T. M., Ed.) pp 239-351, VCH Publishers Inc., New York.
Lineback-Zins, J., & Brew, K. (1980) *J. Biol. Chem. 255*, 708-713.
Mason, A. B., Brown, S. A., Butcher, N. D., & Woodworth, R. C. (1987) *Biochem. J. 245*, 103-109.
Oe, H., Doi, E., & Hirose, M. (1988) *J. Biochem. 108*, 1066-1072.
Schlabach, M. R., & Bates, G. W. (1975) *J. Biol. Chem. 250*, 2182-2188.
Warner, R. C., & Weber, I. (1953) *J. Am. Chem. Soc. 75*, 5094-5101.
Williams, J. (1974) *Biochem. J. 141*, 745-752.
Williams, J., Evans, R. W., & Moreton, K. (1978) *Biochem. J. 173*, 535-542.
Williams, S. C., & Woodworth, R. C. (1973) *J. Biol. Chem. 248*, 5848-5853.
Wiseman, T., Williston, S., Brandts, J. F., & Lin. L.-N. (1989) *Anal. Biochem. 17*, 131-137.
Woodworth, R. C., Virkaitis, L. M., Woodbury, R. G., & Faval, R. A. (1975) in *Proteins of Iron Storage and Transport in Biochemistry and Medicine* (Crichton, R. R., Ed.) pp 39-50, North-Holland Publishing Co., Amsterdam.
Zak, O., & Aisen, P. (1985) *Biochim. Biophys. Acta 829*, 348-353.
Zak, O., Leibman, A., & Aisen, P. (1983) *Biochim. Biophys. Acta 742*, 490-495.

A Totally Synthetic Histidine-2 Ferredoxin: Thermal Stability and Redox Properties†

Eugene T. Smith,‡ John M. Tomich,§ Takeo Iwamoto,§ John H. Richards,∥ Yuan Mao,‡ and Benjamin A. Feinberg*,‡

Department of Chemistry, The University of Wisconsin—Milwaukee, P.O. Box 413, Milwaukee, Wisconsin 53201, Department of Biochemistry, University of Southern California, Childrens Hospital of Los Angeles, P.O. Box 54700, Los Angeles, California 90054-0700, and Division of Chemistry and Chemical Engineering, California Institute of Technology, Pasedena, California 91125

Received May 28, 1991; Revised Manuscript Received September 10, 1991

ABSTRACT: The entire polypeptide of *Clostridium pasteurianum* ferredoxin (Fd) with a site-substituted tyrosine-2 → histidine-2 was synthesized using standard *t*-Boc procedures, reconstituted to the 2[4Fe-4S] holoprotein, and compared to synthetic *C. pasteurianum* and native Fds. Although histidine-2 is commonly found in thermostable clostridial Fds, the histidine-2 substitution into synthetic *C. pasteurianum* Fd did not significantly increase its thermostability. The reduction potential of synthetic histidine-2 Fd was −343 and −394 mV at pH 6.4 and 8.7, respectively, versus standard hydrogen electrode. Similarly, *Clostridium thermosaccharolyticum* Fd which naturally contains histidine-2 was previously determined to have a pH-dependent reduction potential [Smith, E. T., & Feinberg, B. A. (1990) *J. Biol. Chem. 265*, 14371-14376]. An electrostatic model was used to calculate the observed change in reduction potential with pH for a homologous ferredoxin with a known X-ray crystal structure containing a hypothetical histidine-2. In contrast, the reduction potential of both native *C. pasteurianum* Fd and synthetic Fd with the *C. pasteurianum* sequence was −400 mV versus standard hydrogen electrode and was pH-independent [Smith, E. T., Feinberg, B. A., Richards, J. H., & Tomich, J. M. (1991) *J. Am. Chem. Soc. 113*, 688-689]. On the basis of the above results, we conclude that the observed pH-dependent reduction potential for both synthetic and native ferredoxins that contain histidine-2 is attributable to the electrostatic interaction between histidine-2 and iron-sulfur cluster II which is approximately 6 Å away.

The ubiquitous iron-sulfur proteins play essential roles in respiratory, photosynthetic, and fermentative pathways. The electron-transport proteins ferredoxins (Fds)[1] contain [4Fe-4S] clusters that each accept or donate one electron and have a reduction potential of about −400 mV. The ferredoxin (Fd) from *Clostridium pasteurianum*, which was first isolated by Mortenson et al. (1962), is characteristic of other clostridial Fds in that it contains two [4Fe-4S] clusters and has a low molecular weight (6000).

In the elegant work by Rabinowitz and co-workers, semisynthetic procedures were used to chemically substitute or delete specific amino acids near the polypeptide terminus of *Clostridium acidi-urici* ferredoxin (Lode et al., 1974a,b, 1976). The semisynthetic approach was used to demonstrate that the

† This research was supported by a grant to B.A.F. from the National Institutes of Health (GM41927-01) and with funds from the University of Wisconsin—Milwaukee Graduate School.
* To whom correspondence should be addressed.
‡ The University of Wisconsin—Milwaukee.
§ Childrens Hospital of Los Angeles.
∥ California Institute of Technology.

[1] Abbreviations: Fd, ferredoxin, DTT, dithiothreitol; IPA, isopropyl alcohol; *t*-Boc, *tert*-butoxycarbonyl; PAGE, polyacrylamide gel electrophoresis; EPR, electron paramagnetic resonance; SHE, standard hydrogen electrode.

0006-2960/91/0430-11669$02.50/0

aromatic residues typically found near the iron–sulfur clusters were not necessary for electron transfer to occur (Lode et al., 1974a). Subsequent studies revealed that out of 13 *C. acidi-urici* ferredoxin derivatives (Lode et al., 1976), histidine-2 was the *only* stable substitution which resulted in an altered reduction potential. It was concluded that the +15-mV change in reduction potential of histidine-2 *C. acidi-urici* Fd near pH 7 was due to a change in protein conformation (Lode et al., 1976).

Building on the pioneering work of Rabinowitz and coworkers, we recently synthesized the *entire* polypeptide sequence of *C. pasteurianum* Fd, and reconstituted it to the holoprotein (Smith et al., 1991a). The totally synthetic Fd had spectroscopic and redox properties similar to those of native *C. pasteurianum* Fd, and served as a competent electron carrier for hydrogenase. Through this novel approach, we can now examine the effects of specific amino acid substitutions throughout the entire polypeptide. With a totally synthetic ferredoxin, we reexamine the role of histidine-2 which is commonly found in native clostridial Fds. Histidine-2 in native ferredoxins is believed to increase thermostability (Perutz & Raidt, 1975) and to influence equilibrium redox properties (Smith & Feinberg, 1990).

Within the genus *Clostridium*, ferredoxins have been isolated from thermophilic and mesophilic organisms, which grow optimally at 55 and 37 °C, respectively. Although about 60% of the primary structure for clostridial Fds is conserved, thermophilic Fds are moderately heat-stable (Devanathan et al., 1969; Elliott & Ljungdahl, 1982; Bruschi et al., 1986). In many thermophilic clostridial ferredoxins, histidine replaces the aromatic residue typically found at position 2, though the significance of this substitution is not known. It is believed that differences in the free energy of ionization between interior histidine residues in the folded and unfolded conformations make significant contributions to conformational stability (McNutt et al., 1990). The increased thermostability of 2-[4Fe–4S] ferredoxins has been attributed to the interactions of amino acids in the region around the N- and C-terminus (Bruschi et al., 1986, 1991). In general, moderate increases in thermostability in thermophilic proteins have been attributed to additional salt bridges, hydrogen bonds, and hydrophobic interactions (Perutz & Raidt, 1975; Argos et al., 1979), as well as an increase in mobility of hydrophobic interior residues (Alber et al., 1987). However, despite the growing interest in this area, particularly for biotechnical purposes, the molecular basis for thermostability is far from being established.

Despite the numerous studies in the last 2 decades, little is still known about how proteins regulate or influence the redox potential of [4Fe–4S] centers, which differ widely among iron–sulfur proteins. *C. pasteurianum* Fd serves as a good model for testing the influence of ionizable residues on protein functionality since it has (a) no residues ionizing near neutral pH, (b) no measurable spectroscopic changes with pH detected for *C. pasteurianum* Fd (Magliozzo et al., 1982), and (c) a reduction potential that is pH-independent (Prince & Adams, 1987; Smith & Feinberg, 1990). We recently reported that the reduction potentials of native and totally synthetic *C. pasteurianum* Fds were identical, and pH-independent (Smith et al., 1991a).

In contrast, we recently determined that the reduction potential of native histidine-2 *Clostridium thermosaccharolyticum* Fd was pH-dependent (Smith & Feinberg, 1990). The change in reduction potential with pH corresponded to a theoretical model for a single titratable site with a $pK_{ox} \approx 7.0$ and $pK_{red} \approx 7.5$. The magnitude of the change in reduction potential with pH was calculated by Coulomb's law based on an electrostatic interaction between an ionizable histidine-2 and iron–sulfur cluster II. In this paper, we investigate the effect on the redox properties of a totally synthetic *C. pasteurianum* Fd caused by a single substitution of an ionizable residue. We also calculate the electrostatic potentials for a hypothetical protonated versus unprotonated histidine-2 ferredoxin using a dielectric continuum model. This electrostatic model, based on the Poisson–Boltzman equation, has been used to successfully reproduce experimental observations for many proteins [Bashford & Karplus, 1990; see Honig et al. (1986), and Sharp and Honig (1990) and references cited therein].

Materials and Methods

Native Protein Preparation. Clostridium pasteurianum (ATCC 6013) and *Clostridium thermosaccharolyticum* (ATCC 7956) were cultured according to Rabinowitz (1972) and Mercer and Vaughn (1951), respectively, at the University of Wisconsin—Milwaukee and then grown in a 350-L fermentor at the University of Wisconsin—Madison, Department of Biochemistry. The Fds were isolated anaerobically at 4 °C using slight modifications of methods previously described (Rabinowitz, 1972). The purity ratio of $A_{390}/A_{280} = 0.83$, as determined by Rabinowitz (1972), was used as an index of protein purity.

Chemicals for Peptide Synthesis. The reagents and their sources used in peptide synthesis are as follows: *t*-Boc-amino acids (Peninsula Laboratories); *t*-Boc-His-DNP (Fluka); *t*-Boc-aminoacyl-OCH_2-PAM resins (Applied Biosystems Inc.); β-mercaptoethanol, *p*-cresol, *p*-thiocresol, dithiothreitol (DTT), dichloromethane, anhydrous diethyl ether, and acetic acid (Mallinckrodt); diisopropylethylamine trifluoroacetic acid (Aldrich Chemical Co.); acetonitrile, dimethylformamide, *n*-propyl alcohol, tetrahydrofuran, and methanol (all HPLC grade; Burdick and Jackson); anhydrous HF (Mattheson).

Synthetic Ferredoxin. The 55 amino acid sequence of *C. pasteurianum* Fd is (Tanaka et al., 1966) A[1]YKIADSCVSC[11]GACASECPVN[21]AISQGDSIFV[31]IDADTCIDCG[41]NCANVCPVGA[51]PVQE. The synthetic histidine-2 Fd has the same sequence except tyrosine-2 is substituted with histidine. The synthetic polypeptide was synthesized using PAM resins and an automated solid-phase protocol, based on the principles outlined by Merrifield (1963, 1965), on an Applied Biosystems Model 430 peptide synthesizer. To ensure a high degree of coupling efficiency, all amino acids were coupled 2–4 times.

For the synthetic histidine-2 sequence which contained a dinitrophenyl protecting group, histidine thiolysis was performed. The peptide resin (0.25 g) was treated twice for 30 min at 25 °C with 15 mL of 10% diisopropylethylamine/20% β-mercaptoethanol in dimethylformamide to remove the dinitrophenol protecting group.

The N^{α}-*t*-Boc group was subsequently removed with 65% trifluoroacetic acid (TFA) for 10 min at 25 °C. The polypeptide/resin was dried and immediately treated with anhydrous HF. Cleavage and full deprotection of the polypeptide were carried out using 0.45 g of the pretreated peptide/resin in the presence of 0.65 mL of scavenger (*p*-cresol), 0.33 mL of reducing agent (*p*-thiocresol), and 8–10 mL of anhydrous HF. The HF was condensed at −40 °C, and the reaction was allowed to proceed for 30 min at −10 °C and 60 min at 0 °C employing an Immuno-Dynamics HF cleavage apparatus. Liquid HF was removed at the end of the reaction, and the cleavage reaction mixture was washed with 100 mL of cold anhydrous diethyl ether. The resultant precipitate which contained the cleaved peptide and vinylbenzene resin was

collected and dried in vacuo over KOH.

The polypeptide was separated from the vinylbenzene resin by dissolving 100 mg of the polypeptide/resin precipitate into 50 mL of 5% sodium trichloroacetic acid/100 mM Tris, pH 8, and filtered through 0.2-μm hydrophilic nylon membranes (Lida Manufacturing Corp., Kenosha, WI). The trichloroacetic acid was removed through dialysis in 100 mM Tris, pH 8.

Amino Acid Sequence. The amino acid sequence of the synthetic peptide was determined by utilizing an Applied Biosystems Model 477 peptide sequencer using resin samples taken during and after synthesis.

Gel Electrophoresis. Two milligrams of native and synthetic apoprotein with the native sequence was permitted to migrate in tube gels for 2 days at 350 V. The stacking gel was 0.5% bis(acrylamide), 2.2% acrylamide, and 70 mM Tris, pH 6.9. The separating gel was 0.2% bis(acrylamide), 4.5% acrylamide, and 215 mM Tris, pH 8.5. The proteins were fixed to the gels with 12% TCA for 8 h, neutralized with 2% Na_2CO_3, stained with 0.2% Coomassie Blue for 12 h, and destained with 7% acetic acid and 5% methanol.

HPLC. A 1.0-mL sample of native and synthetic apoprotein was chromatographed at 61 °C on a two-pump HPLC fitted with a TOSOH TSK Gel C_{18}-4PW column (7-μm particle size, 4.6 mm × 150 mm). The apoprotein was chromatographed with 10% isopropyl alcohol (90% isopropyl alcohol/0.1% TFA) for 2 min, followed by a 10–90% isopropyl alcohol gradient over 40 min. The optical densities of native and synthetic apoprotein at 225 nm were 1.0 and 0.35, respectively.

Cluster Reconstitution. The iron–sulfur clusters were reconstituted using a procedure developed in this laboratory based on a previously reported protocol (Rabinowitz, 1972). The apoprotein, which was separated from the PAM resin as described above, was incubated anaerobically in a 20-fold molar excess of DTT and then dialyzed in 100 mM Tris, pH 8, for 24 h to remove DTT. Then 50-fold molar excess of $FeCl_3$ and Na_2S was added, and the mixture was incubated anaerobically at 25 °C for 3 h. The solution was passed over a DE-52 column (1 cm × 2 cm) equilibrated to 50 mM Tris, pH 8, washed with buffer, and eluted with 0.5 M NaCl. The holoprotein was further purified on a column fabricated in the lab (0.5 cm × 10 cm) using QDE [diethyl-(2-hydroxypropyl)aminoethyl]-Sepharose equilibrated to 50 mM Tris, pH 8, by salt gradient chromatography (100 mL of 50 mM Tris, pH 8, and 0–0.5 M NaCl).

Electron Paramagnetic Resonance. EPR spectra were recorded on a Varian Model E115 spectrometer with an automatic frequency counter (Model 548A, EIP Microwave, Inc.). The temperature was maintained near 10 K with a liquid helium cryogenic system (Heli-Tran Model LTD-3-110, APD Cryogenics Co.). The digital readout on the Air Products unit had been calibrated with a calibrated gold thermocouple. All samples which were in 50 mM Tris, pH 8, and 0.1 M NaCl were reduced by dithionite.

Thermostability. Since [4Fe–4S] clusters absorb strongly in the visible region due to FeS charge transfer bands, these clusters serve as an excellent internal probe into the stability of the protein. The Fds were anaerobically placed in 1-mL quartz cuvettes containing 50 mM buffer (phosphate, pH 6–7; Tris, pH 8–9), and the ionic strength was adjusted with solid NaCl. The bleaching of the FeS chromophore with time at 70 °C was measured spectroscopically at 390 nm as previously described (Devanathan et al., 1969). This method has been routinely used to determine the thermostability of bacterial ferredoxins (Devanathan et al., 1969; Elliot & Ljungdahl, 1982; Bruschi et al., 1986; Hatchikian et al., 1989). All visible spectra in this paper were recorded on a computer-interfaced Cary 219 spectrophotometer with thermostated cell compartments.

Reduction Potentials. All proteins were dialyzed anaerobically in the appropriate buffer (cacodylic, pH 6.4; phosphate, pH 6.4–6.7; Tris, pH 8.0–8.7) for 24 h at 4 °C. Concentrated stock solutions of all the proteins in the appropriate buffer were diluted into the various supporting electrolytes. The specific concentrations of the electrolytes ($MgCl_2$ and NaCl) used to maximize protein–electrode interactions were based on a previous protocol (Armstrong et al., 1987). All square-wave voltammetric experiments were performed using a standard three-electrode configuration as previously described (Smith et al., 1991b). The cell was made anaerobic by cycling between a vacuum and purified argon passed over a heated R3-11 catalyst (Chemical Dynamics Corp., South Plainfield, NJ). An anaerobic 25-μL sample containing 30–100 μM synthetic Fd in the appropriate buffer and supporting electrolyte was placed on the inverted working electrode via a Hamilton gas-tight syringe. All current/potential data from the electrochemical experiments were gathered using either a computer-interfaced PARC 273 or a BAS-100 potentiostat. Equilibrium reduction potentials were determined from the voltammograms at the applied potential at which the peak current occurred. The number of electrons transferred per redox center was determined from the peak width at half-height ($W_{1/2} = 126$ mV/n). All potentials in this paper are reported versus SHE.

Electrostatic Potential Calculations. In this study, electrostatic interaction energies were calculated using the Poisson–Boltzmann equation which allows for the spatial variation of charge density and dielectric constant. The reader is referred to two excellent review articles which detail the theory behind dielectric continuum electrostatic calculations [see Honig et al. (1986) and Sharp and Honig (1990) and references cited therein]. The Poisson equation is expressed as

$$\vec{\nabla}[\epsilon(r)\vec{\nabla}\Phi(r)] = 4\pi\rho(r) \quad (1)$$

where $\Phi(r)$ is the electrostatic potential, $\epsilon(r)$ is the dielectric constant, and $\rho(r)$ is the charge density, all as a function of position. The electrostatic interaction energy attributed to solvated ions based on Debye–Huckel theory is easily incorporated into eq 1 to obtain the Poisson–Boltzmann equation:

$$\vec{\nabla}[\epsilon(r)\vec{\nabla}\Phi(r)] - \kappa^2\epsilon(r)\Phi(r)[1 + \lambda\Phi^2(r)] + 4\pi\rho(r) = 0 \quad (2)$$

where λ is $e^2/6k^2T^2$, κ^2 is $(8\pi e^2NI)\epsilon kT$, N is Avogadro's constant, I is the ionic strength, and k is the Boltzmann constant.

Charge Density. The coordinates for *Peptococcus aerogenes* Fd, which has over 70% homology with *C. pasteurianum* Fd, as determined from the X-ray crystal structure (Adman et al., 1973) were obtained from the Brookhaven Data Bank (Bernstein et al., 1977). Coordinates of the ϵ-carbons of tyrosine-2 were used as an approximation to the positions of imidazole nitrogens for the hypothetical histidine-2. Hydrogen atoms were not explicitly included in the calculations.

The net atomic charges used in the electrostatic potential calculations for amino acid side chains and backbone atoms were calculated from molecular mechanical simulations (Weiner et al., 1984). Net atomic charge sets for [4Fe–4S] clusters that were examined include those calculated by LCAO-Xα valence scattered wave (Noodleman et al., 1985) and LCAO-Xα broken symmetry (Noodleman, personal communication) methods.

Dielectric Constant. The dielectric constant is spatial average accounting for the response of the medium to the fields generated by the charge distribution. This parameter represents the shielding of charge interactions due to electronic polarization, reorientation of permanent dipoles, and redistribution of charges, e.g., electric double layer. Since the protein dielectric constant cannot readily be determined experimentally and may be protein-dependent, it is difficult to assign the appropriate value for the protein dielectric constant (Warshel, 1987; Gilson & Honig, 1988).

It has been suggested that ferredoxins may have a relatively high protein dielectric constant due to the permanent dipolar interactions of hydrogen bonds between the cluster and backbone amides (Kassner & Yang, 1977). The low molecular weight ferredoxins, which contain no secondary structure (e.g., α-helices), provide an unusual protein environment for their redox centers since the clusters are not surrounded by hydrophobic residues and are relatively exposed to solvent. As many as 18 hydrogen bonds can form between backbone amides and cysteinyl sulfur atoms which make up the cluster (Adman et al., 1975).

In this application, the dielectric constant is assigned to two distinct regions, the solvent with a dielectric constant of 80 and the protein with a dielectric constant of 20. This value of the protein dielectric constant was previously used in calculations which accurately reproduced experimentally observed (Smith et al., 1991b) free energy differences for ferredoxin. For example, the reduction potential of Fds was determined to be dependent on ionic strength (Lode et al., 1976; Prince & Adams, 1987). Their experimental results were reproduced by electrostatic calculations (Smith et al., 1991b) using the identical parameter sets as used in this study.

Finite Difference Technique. Electrostatic potentials were calculated on a Silicon Graphics System (IRIS Model 4D/70G) using a commercially available version of DELPHI (Copyright Columbia University, 1987). In DELPHI, a finite difference solution to the Poisson–Boltzmann equation is used to numerically solve for the electrostatic potential. Numerical solutions to the Poisson–Boltzmann equation were determined to be within 5–15% of analytical solutions (Gilson et al., 1987). The protein was mapped onto a three-dimensional grid of atomic resolution. The grid size and spacing were chosen to maximize protein resolution and to allow for an accurate description of the potential energy at the grid boundary. In this application, the protein filled 60% of a three-dimensional grid (65 × 65 × 65), and the grid spacing was 1.1 grids/Å.

The dielectric constant, charge density, and ionic strength parameters were assigned to each grid point. The ionic strengths used in the electrostatic calculations were identical to those used in the experimental determinations of the reduction potentials. The electrostatic potential was calculated at each grid point, and the potentials were summed over the entire grid. The net electrostatic potential energy between the ferredoxin in both oxidation states was calculated and subtracted from the net electrostatic potential energy calculated between both oxidation states of the ferredoxin containing a hypothetical protonated histidine-2.

RESULTS

Protein Characterization. The amino acid sequence of the synthetic Fds was confirmed during and after synthesis. The measured weight gain for the synthesis was 82.9% of the theoretical weight gain, which translates to an average coupling yield of 99.7% per residue. The synthetic apoprotein with the native sequence and the native apoprotein bands eluted to identical positions on PAGE gels after 48 h of electrolysis.

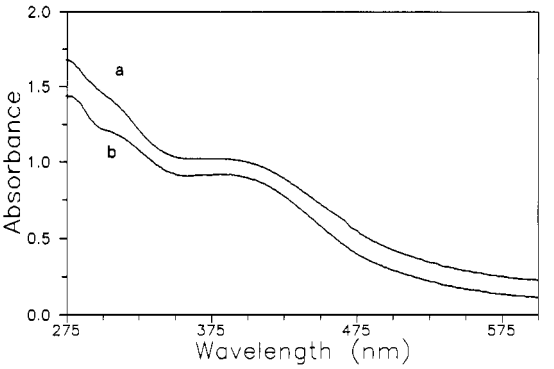

FIGURE 1: UV–visible spectra of 30 μM (a) native *C. pasteurianum* Fd and (b) synthetic histidine-2 *C. pasteurianum* Fd in 0.1 M NaCl and 50 mM Tris, pH 8. Spectra are offset 0.01 absorbance unit.

Table I: Reported g Values from EPR Spectra of Synthetic and Native Ferredoxins

	g_x	g_y	g_z	reference
histidine-2 *C. pasteurianum*	1.89	1.94	2.05	this work
C. thermoaceticum	1.89	1.92	2.05	Elliot & Ljungdahl (1982)
synthetic *C. pasteurianum*	1.91	1.94	2.06	Smith et al. (1991a)
native *C. pasteurianum*	1.89	1.94	2.05	Orme-Johnson & Beinert (1969)

Table II: Percent Denatured Ferredoxin after 1 h at 70 °C as a Function of Ionic Strength (50 μM Fd in 50 μM Tris, pH 8)

ionic strength	*C. pasteurianum*	*C. thermosaccharolyticum*
0.01	25.8	10.6
0.025	18.5	10.0
0.05	12.0	11.9
0.10	10.2	8.0
0.25	8.0	7.2
0.50	8.0	6.5

Table III: Percent Denatured Ferredoxin after 1 h at 70 °C as a Function of pH (50 μM in 50 mM Tris/0.1 M NaCl)

pH	*C. pasteurianum*	*C. thermosaccharolyticum*
6.0	20.8	7.8
7.0	16.5	6.0
8.0	10.0	10.0
9.0	13.0	11.0

Native holoprotein was clearly separated from the apoprotein under the same conditions after 12 h. It was determined from HPLC that both native and synthetic apoprotein had an identical retention time of 45.4 s. From 75 mg of PAM resin/synthetic apoprotein, about 7.5 mg of the reconstituted synthetic protein with a purity ratio (A_{390}/A_{280}) greater than 0.8 was obtained.

Spectroscopic Properties. The visible spectra of the oxidized native and synthetic histidine-2 ferredoxin with the native sequence are shown in Figure 1. Both the visible spectra of synthetic ferredoxin (Smith et al., 1991a) and *C. thermosaccharolyticum* Fd which contains a naturally occurring histidine-2 (Smith & Feinberg, 1990) are similar to those found in Figure 1. The spin-coupled [4Fe–4S] clusters of reduced ferredoxins yield complex EPR spectra as shown in Figure 2 for the synthetic histidine-2 ferredoxin. The principal g values for various synthetic and native Fds are listed in Table I.

Thermostability. Plots of denaturation with time at 70 °C for synthetic holoprotein with the native *C. pasteurianum* sequence, synthetic histidine-2, native *C. pasteurianum*, and *C. thermosaccharolyticum* Fds are all shown in Figure 3. The thermophilic *C. thermosaccharolyticum* Fd was found to be

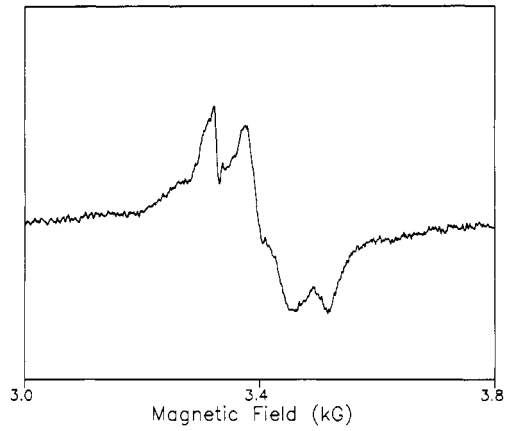

FIGURE 2: X-Band electron paramagnetic resonance spectra of dithionite-reduced 0.2 mM synthetic histidine-2 Fd in 0.1 M NaCl and 50 mM Tris, pH 8. Experimental conditions were the following: microwave power, 0.05 mW; modulation amplitude, 10 G; scan rate, 240 G/min; time constant, 0.25 s; temperature, 16 K; and microwave frequency, 9.317 GHz.

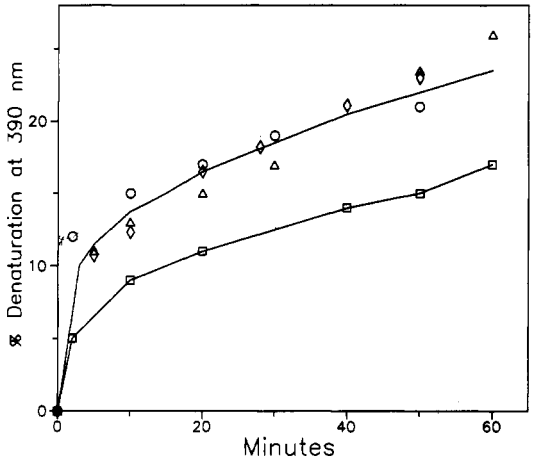

FIGURE 3: Percent denaturation of 30 μM Fd with time at 70 °C in 50 mM Tris, pH 8, where the Fd is (○) native *C. pasteurianum*, (△) synthetic with the native sequence, (◇) synthetic histidine-2 variant, and (□) native *C. thermosaccharolyticum*. No NaCl is present in contrast to the experiments shown in Table III.

about 8 ± 3% more stable after 1 h than the other three ferredoxins that were examined. The percent denaturation of native mesophilic and thermophilic ferredoxins after 1 h as a function of ionic strength is listed in Table II, and percent denaturation as a function of pH is listed in Table III. The results in Tables II and III for native Fds are quite helpful in designing experiments for further synthetic variants, which so far have been obtained in limited quantity.

Reduction Potentials. A typical experimental voltammogram for synthetic histidine-2 Fd at pH 8.7 is shown in Figure 4. It was determined from the peak width at half-height of the voltammogram than one electron was transferred per redox site (n = 1) for all the ferredoxins examined. The broadening of the peak width, which was observed at both pHs for synthetic Fd, is typical of redox couples that exchange electrons at an electrode surface at rates relatively slower than if they were reversible. The reduction potentials of native and synthetic histidine-2 Fds as determined directly at an edge pyrolytic graphite electrode are listed in Table IV. The shift in reduction potential between the pH extremes for synthetic histidine-2 Fd (51 mV) is in the same direction and of similar magnitude as the shift of 30 mV for *C. thermosaccharolyticum* Fd, which has histidine-2. The pK_{ox} and pK_{red} of the histidine-2 variant, requiring a full pH–$E^{\circ\prime}$ study, were not determined

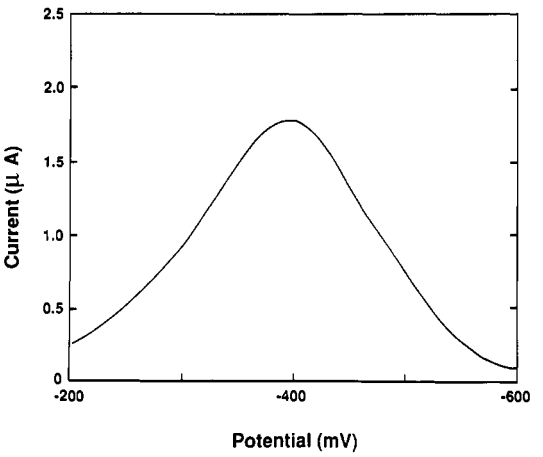

FIGURE 4: Square-wave voltammogram at an edge pyrolytic graphite electrode for 25 μL of 100 μM synthetic Fd in 50 mM Tris, pH 8, adjusted to an ionic strength of 0.1 with $MgCl_2$. The experimental conditions were as follows: pulse potential = 50 mV, step potential = 4 mV, and applied pulse frequency = 4 Hz.

Table IV: Equilibrium Reduction Potentials (mV) of Native and Synthetic Ferredoxins[a]

	$E^{\circ\prime}_{pH6.4}$	$E^{\circ\prime}_{pH8.7}$
C. pasteurianum	−400	−404
synthetic *C. pasteurianum*	−403	−395
C. thermosaccharolyticum	−382	−412
histidine-2 *C. pasteurianum*	−343	−394

[a] average experimental uncertainty was ±5 mV.

Table V: Calculated ΔE between Ionization States for Histidine-2 Ferredoxin for Different Net Atomic Charge Sets of Iron–Sulfur Clusters

LCAO-Xα method	ΔE (mV)[a]
valence scattered wave	48
broken symmetry, oxidized geometry	57
broken symmetry, relaxed geometry	57

[a] A protein dielectric constant of 20 was used. Protein net atomic charge sets were those calculated by Noodleman et al. (1986) and Noodleman (personal communication).

due to the low yield of holoprotein from the synthetic apoprotein. The calculated electrostatic potential differences between ionization states of a hypothetical histidine-2 Fd as a function of different net atomic charge sets are listed in Table V. The observed differences in reduction potential for both the native and synthetic histidine-2 Fds are in reasonable agreement with the calculated electrostatic potential differences between ionization states of a hypothetical histidine-2.

Discussion

Although the formation of iron–sulfur clusters is thermodynamically favorable, some difficulties were encountered during in vitro reconstitution of the synthetic ferredoxin, possibly due to either unfavorable conformations of the polypeptide or the formation of high molecular weight aggregates through intermolecular disulfide bonds. As mentioned previously (Smith et al., 1991a), synthetic Fd differs significantly from previous $[4Fe–4S]^{2+/1+}$ analogues in the way the clusters are ligated, and from native protein in the way it is synthesized and reconstituted. We are currently working on ways to improve yields, including the use of protecting groups on cysteine. Preliminary results in this laboratory using an acetamidomethyl protecting group (Veber et al., 1972) are encouraging.

Despite our novel approach to protein synthesis and reconstitution, no distinction could be made between the native

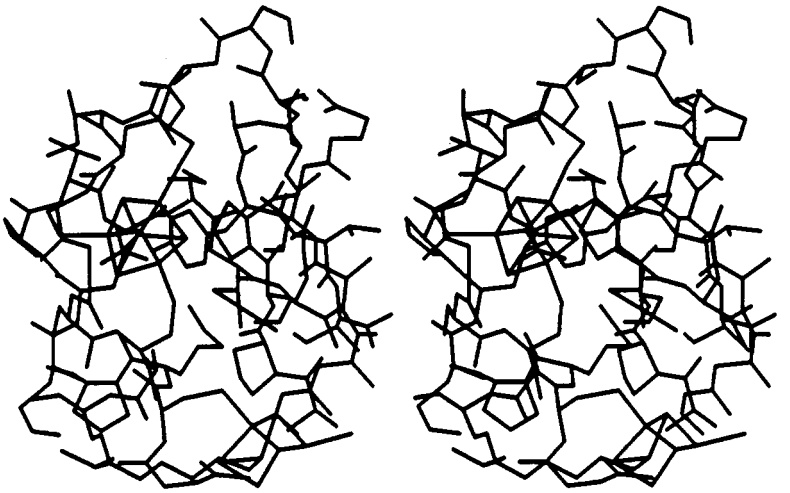

FIGURE 5: Stereo figure showing the amino acid side chains within 12 Å of Fe 2 of cluster II based on the X-ray crystal structure of *P. aerogenes* ferredoxin (Adman et al., 1973). Tyrosine-2 is found between and parallel to both proline-52 and the face of the cluster.

and synthetic apoprotein through PAGE gels and amino acid sequencing. Furthermore, it was previously shown (Smith et al., 1991a) that the synthetic Fd after reconstitution has virtually identical redox properties, EPR, circular dichroic, and UV–visible spectra as those of native Fd. In this work, we determined from HPLC that the native and synthetic apoprotein had identical retention times. The visible spectra of site-substituted histidine-2 Fd were found similar to those of native Fds as shown in Figure 1. The EPR spectra of reduced synthetic histidine-2 Fd are shown in Figure 2. The principal *g* values determined for reduced synthetic histidine-2 Fd are in excellent agreement with the *g* values previously determined for other reduced native and synthetic Fds as shown in Table I.

Our results demonstrate that site-substituted ferredoxin variants can be obtained with relative ease through the use of totally synthetic methods. The totally synthetic approach provides advantages over semisynthetic methods (Lode et al., 1976a,b) in that amino acids can be substituted at any position in the primary structure. Although our current yields of holoprotein are not very high, in the future pure apoprotein variants may be totally synthesized, reconstituted, and purified within 1 week. In contrast, the gene for *C. pasteurianum* Fd was poorly transcribed in *Escherichia coli*, with the ferredoxin comprising less than 1% of the total cell protein after purification (Bauer et al., 1990), and no site mutations were examined. We believe that totally synthetic methods will eventually provide advantages over microbiological techniques, including reduced time and expense. In addition, with totally synthetic methods, isotopically labeled or chemically modified amino acids may be easily and specifically incorporated into the primary structure of a protein.

Thermostability. The results shown in Tables II and III for native ferredoxins are quite helpful in determining which experiments should be done with Fd variants that are now being prepared. The thermostability of native *C. thermosaccharolyticum* Fd, although relatively higher than that of *C. pasteurianum* Fd, does not appear to follow the ionization of histidine-2 as shown in Table III. These results also suggest that histidine-2 is not involved in *C. thermosaccharolyticum* Fds increased thermostability. Results in Table III indicate that the thermostability of *C. pasteurianum* Fd appears to be only sensitive at pH extremes in agreement with results obtained by Maskiewicz and Bruice (1977) on acid/base-catalyzed cluster dissolution.

The results presented in Table II suggest that the increased thermostability of *C. thermosaccharolyticum* Fd may be attributed to additional salt bridges, since the protein is not as sensitive to denaturation at low ionic strength as mesophilic *C. pasteurianum* Fd. Perutz and Raidt (1975) have suggested that as many as six additional salt bridges may contribute to the increased thermostability of two thermophilic Fds. Our study indicates that one of the proposed salt bridges (that between histidine-2 and cysteine-43) does not appear to increase thermostability in a mesophilic Fd. We are currently investigating the role of other possible salt bridges.

The role of histidine in increased thermostability has been previously suggested (Perutz & Raidt, 1975; McNutt et al., 1990). However, our thermal denaturation studies indicate that the increased thermostability of thermophilic clostridial Fds probably does not arise from the single substitution of an aromatic residue with histidine-2 (see Figure 3). The residues at positions 2 and 52 appear to be stacked in many mesophilic clostridial Fds, on the basis of a known X-ray structure (see Figure 5). We suggest that these residues play an important role in the folding of the peptide in the critical region near the N- and the C-terminus. A comparison of over 10 homologous Fd sequences (Table VI) indicates that the histidine-2 substitution does not occur without also substituting the amino acid residue at position 52, usually by valine. Interestingly, the amino acid residue found parallel to the face of cluster I

Table VI: Comparison of Amino Acid Sequences of Bacterial Ferredoxins

bacterial species	amino acid[a] 2	30	52	reference
	(A) Mesophiles			
C. pasteurianum	Tyr	Phe	Pro	Tanaka et al. (1966)
C. acidi-urici	Tyr	Tyr	Pro	Rall et al. (1969)
C. butyricum	Phe	Phe	Pro	Benson et al. (1967)
C. perfringens	Tyr	Phe	Pro	Seki et al. (1989)
C. M-E	Tyr	Arg	Ile	Tanaka et al. (1974)
P. aerogenes	Tyr	Tyr	Pro	Tsunoda et al. (1968)
Megasphaera elsdenii[b]	His	Tyr	Ile	Yasunobu & Tanaka (1973)
	(B) Thermophiles			
C. thermosaccharolyticum	His	Tyr	Val	Tanaka et al. (1971)
C. tartarivorum	His	Tyr	Val	Tanaka et al. (1971)
C. thermoaceticum	His	Tyr	Val	Ragsdale (personal communication)
C. thermocellum	Tyr	Tyr	Pro	Bruschi et al. (1986)

[a] Sequence numbering when aligned with *C. pasteurianum* Fd. [b] Formerly *Peptostreptococcus elsdeni*.

in most bacterial Fds is *not* histidine, and *not* stacked between the face of the cluster and another amino acid residue. The packing of amino acid side chains in this region may be an important factor in the mechanism of unfolding of the polypeptide at elevated temperatures as previously suggested (Bruschi et al., 1986, 1991).

Reduction Potentials. The peak width of the voltammograms of both native (Smith & Feinberg, 1990) and synthetic Fds containing histidine-2 was determined to be pH-independent. It appears that the reduction potential of both clusters is affected by the ionization of histidine-2, despite the distance between histidine-2 and cluster I. Since the square-wave voltammogram (SWV) is not split or unusually broadened, the clusters are apparently not affected differentially. In this light, the observed reduction potential is not the average potential of the two clusters but rather reflects the summation of all electrostatic interactions in the protein on both clusters. In the case of histidine-2 Fds, the redox couple is not proton-linked but is indirectly influenced by the nearby ionizable residue. For a redox couple with an *obligatory* proton exchange (e.g., $H^+ + OX + e^- \rightleftharpoons H^+red^-$), a 59 mV/pH unit shift in reduction potential is observed because the difference between pK_{ox} and pK_{red} is very large.

In our previous paper (Smith & Feinberg, 1990), the difference in electrostatic potential energy between ionization states of histidine-2 in *C. thermosaccharolyticum* Fd was estimated from Coulomb's law, which is an analytical solution to the Poisson–Boltzmann equation for a single dielectric constant. By partitioning the electrostatic interactions of histidine-2 and iron–sulfur cluster II from all other electrostatic interactions, Coulomb's law was applicable. Our previous calculation, however, did not take into account other charge–charge interactions or the heterogeneity of dielectric constant. In this paper, we utilize a numerical solution to the Poisson–Boltzmann equation to account for the spatial variation of both charge density and dielectric constant. These calculations account for additional charge–charge interactions and the heterogeneity of the dielectric constant. Both the previous calculation based on Coulomb's law (Smith & Feinberg, 1990) and the electrostatic calculation based on the Poisson–Boltzmann equation (see Table V) suggest that the electrostatic interaction between a single charged residue located near iron–sulfur cluster II may affect the observed reduction potential.

In summary, this study indicates that the presence of histidine-2 in thermophilic clostridial ferredoxins in itself does not explain their increased thermostability. We predict from sequence homologies shown in Table VI that increased thermostability in thermophilic clostridial ferredoxins is partially due to the histidine-2/valine-52 configuration, which is in a critical region for folding of the polypeptide near iron–sulfur cluster II. In addition, the reduction potential of clostridial Fds which contain histidine-2 is apparently influenced by its ionization state. The observed change in the reduction potential of both synthetic and native Fds that contain histidine-2 can be modeled by electrostatic calculations when reasonable parameters are chosen for the protein dielectric constant and net atomic charges in the clusters.

Acknowledgments

We thank Dr. D. W. Bennett and Dr. D. G. Nettesheim (Department of Chemistry, University of Wisconsin—Milwaukee) for their assistance in the electrostatic potential calculations, C. M. Gorst (Department of Chemistry, University of Wisconsin—Milwaukee) for her assistance in obtaining EPR spectra, Dr. J. E. Wampler (Department of Biochemistry, University of Georgia) for generating the stereo image in Figure 5, and Dr. L. Noodleman (Scripps Research Clinic, La Jolla, CA) for providing the calculated iron–sulfur cluster charge sets prior to publication.

Registry No. Fd, 12321-45-8; histidine-2 Fd, 137028-38-7.

References

Adman, E. T., Sieker, L. C., & Jensen, L. H. (1973) *J. Biol. Chem. 248*, 3987–3996.

Adman, E., Watenpaugh, & Jensen, L. H. (1975) *Proc. Natl. Acad. Sci. U.S.A. 72*, 4854–4858.

Alber, T., Dao-pin, S., Nye, J. A., Muchmore, D. C., & Matthews, B. W. (1987) *Biochemistry 26*, 3754–3758.

Armstrong, F. A., Cox, P. A., Hill, H. A. O., Lowe, V. J., & Oliver, B. N. (1987) *J. Electroanal. Chem. 217*, 331–366.

Argos, P., Rossman, M. G., Grau, U. M., Zuber, H., Frank, G., & Tratschin (1979) *Biochemistry 18*, 5698–5703.

Bashford, D., & Karplus, M. (1990) *Biochemistry 29*, 10219–10225.

Bauer, J. R., Graves, M. C., Feinberg, B. A., & Ragsdale, S. W. (1990) *Biofactors 2*, 191–203.

Benson, A. M., Mower, H. F., & Yansunobu, K. T. (1967) *Arch. Biochem. Biophys. 121*, 563–575.

Bernstein, F. C., Koetzle, T. F., Williams, G. J. B., Meyer, E. F., Jr., Brice, M. D., Rodgers, J. R., Kennard, O., Shimanouchi, T., & Tasumi, M. (1977) *J. Mol. Biol. 112*, 535–541.

Brushi, M., Cambillau, C., Bovier-Lapierre, G., Bonicel, J., & Forget, P. (1986) *Biochim. Biophys. Acta 873*, 31–37.

Brushi, M., Bonicel, J., Hatchikian, E. C., Fardeau, M. L., Belaich, J. P., & Frey, M. (1991) *Biochim. Biophys. Acta 1076*, 79–85.

Devanathan, T., Akagi, J. M., Hersh, R. T., & Himes, R. H. (1969) *J. Biol. Chem. 244*, 2846–2853.

Elliott, J. I., & Ljungdahl, L. G. (1982) *J. Bacteriol. 151*, 328–333.

Gilson, M. K., & Honig, B. H. (1988) *Proteins: Struct., Funct., Genet. 3*, 32–52.

Gilson, M. K., Sharp, K. A., & Honig, B. H. (1987) *J. Comput. Chem. 9*, 327–335.

Hatchikian, E. C., Fardeau, M. L., Bruschi, M., Belaich, J. P., Chapman, A., & Cammach, R. (1989) *J. Bacteriol. 171*, 2384–2390.

Honig, B. H., Hubbell, W. L., & Flewelling, R. F. (1986) *Annu. Rev. Biophys. Biophys. Chem. 15*, 163–193.

Kassner, R. J., & Yang, W. (1977) *J. Am. Chem. Soc. 99*, 4351–4355.

Lode, E. T., Murray, C. L., & Rabinowitz, J. C. (1974a) *Biochem. Biophys. Res. Commun. 61*, 163–169.

Lode, E. T., Murray, C. L., Sweeney, W. V., & Rabinowitz (1974b) *Proc. Natl. Acad. Sci. U.S.A. 71*, 1361–1365.

Lode, E. T., Murray, C. L., & Rabinowitz, J. C. (1976) *J. Biol. Chem. 251*, 1683–1687.

Magliozzo, R. S., McIntosh, B. A., & Sweeney, W. V. (1982) *J. Biol. Chem. 257*, 3506–3509.

Maskiewicz, R., & Bruice, T. C. (1977) *Biochemistry 16*, 3024–3029.

McNutt, M., Mullins, L. S., Raushel, F. M., & Pace, N. C. (1990) *Biochemistry 29*, 7572–7576.

Mercer, W. A., & Vaughn, R. H. (1951) *J. Bacteriol. 62*, 27–37.

Merrifield, R. B. (1963) *J. Am. Chem. Soc. 85*, 2149.

Merrifield, R. B. (1965) *Science 150*, 178–185.

Mortenson, L. E., Valentine, R. C., & Carnahan, J. E. (1962) *Biochem. Biophys. Res. Commun. 7*, 448–452.

Noodleman, L., Norman, J. G., Osborne, J. H., Aizman, A., & Case, D. A. (1985) *J. Am. Chem. Soc. 107*, 3418–3426.
Orme-Johnson, W. H., & Beinert, H. (1969) *Biochem. Biophys. Res. Commun. 36*, 337–344.
Perutz, M. F., & Raidt, H. (1975) *Nature 255*, 256–259.
Prince, R. C., & Adams, M. W. W. (1987) *J. Biol. Chem. 262*, 5125–5128.
Rabinowitz, J. (1972) *Methods Enzymol. 24*, 431–446.
Rall, S. C., Bolinger, R. E., & Cole, R. D. (1969) *Biochemistry 8*, 2486–2496.
Seki, Y., Seki, S., & Ishimoto, M. (1989) *J. Gen. Appl. Microbiol. 35*, 167–172.
Sharp, K., & Honig, B. (1990) *Annu. Rev. Biophys. Biophys. Chem. 19*, 301–332.
Smith, E. T., & Feinberg, B. A. (1990) *J. Biol. Chem. 265*, 14371–14376.
Smith, E. T., Feinberg, B. A., Richards, J. H., & Tomich, J. M. (1991a) *J. Am. Chem. Soc. 113*, 688–689.
Smith, E. T., Bennett, D. W., & Feinberg, B. A. (1991b) *Anal. Chim. Acta 251*, 27–33.
Tanaka, M., Nakashima, T., Benson, A. M., Mower, H. F., & Yansunobu, K. T. (1966) *Biochemistry 5*, 1666–1681.
Tanaka, M., Mitsuru, H., Matsueda, G., Yasunobu, K. T., Himes, R. H., Akagi, J. M., Barnes, E. M., & Devanathan, T. (1971) *J. Biol. Chem. 246*, 3953–3960.
Tanaka, M., Mitsuru, H., Matsueda, G., Yasunobu, K. T., Jones, J. B., & Stadtman, T. C. (1974) *Biochemistry 13*, 5284–5289.
Tsunoda, J. N., Yasunobu, K. T., & Whiteley, H. R. (1968) *J. Biol. Chem. 243*, 6262–6272.
Veber, D. F., Milkowski, J. D., Varga, S., Denkewalter, R. G., & Hirschman, R. (1972) *J. Am. Chem. Soc. 94*, 5416.
Warshel, A. (1987) *Nature 330*, 15–17.
Weiner, S. J., Kollman, P. A., Case, D. A., Singh, U. C., Ghio, C., Alagoma, G., Profeta, S., Jr., & Weiner, P. (1984) *J. Am. Chem. Soc. 106*, 765–784.

A Synthetic Peptide of the N-Terminus of Actin Interacts with Myosin†

Jennifer E. Van Eyk and Robert S. Hodges*

Department of Biochemistry and MRC Group in Protein Structure and Function, University of Alberta, Edmonton, Alberta T6G 2H7, Canada

Received November 19, 1990; Revised Manuscript Received August 19, 1991

ABSTRACT: Research reported from numerous laboratories suggested that the N-terminal region of actin contained one of the binding sites between actin and myosin. A synthetic peptide corresponding to residues 1–28 of skeletal actin was prepared by solid-phase peptide methodology. The formation of a complex between this peptide and myosin subfragment 1 (S1) was demonstrated by high-performance size-exclusion chromatography (pH 6.8). The actin peptide precipitated S1 at higher pH (7.4–8.2) but remained soluble when bound to heavy meromyosin (HMM) or S1 in the presence of F-actin. The actin peptide 1–28 bound to S1 and HMM and activated the ATPase activity in a manner similar to that of F-actin. These results demonstrate that the N-terminal region of actin, residues 1–28, contains a biologically important binding site for myosin.

The use of synthetic peptides that mimic biologically important regions of proteins has been extremely informative in investigating complex biological systems. For example, the studies by Talbot and Hodges (1979) initiated extensive synthetic peptide research on muscle proteins that has contributed to our understanding of the mechanism of muscle contraction (Suzuki et al., 1987; Van Eyk & Hodges, 1988; Shaw et al., 1990; Keane et al., 1990). Muscle contraction involves the regulation of the actin and myosin (acto–myosin) interaction by the regulatory protein complex, troponin–tropomyosin (Tn–TM). The troponin (Tn) subunits (TnC, TnI, TnT) interact with each other and work in concert with actin–TM to produce conformational changes which alter the acto–myosin interaction. When either Mg^{2+} or Ca^{2+} is bound to the two high-affinity Ca^{2+}-binding sites of TnC, muscle relaxation is promoted due to the induction of inhibition of the ATPase activity by TnI (Van Eyk et al., 1986). In contrast, Ca^{2+} binding to the two low-affinity Ca^{2+}-binding sites of TnC results in muscle contraction due to the release of TnI inhibition and potentiation of the ATPase activity.

Immunological data, cross-linking, and NMR experiments have strongly indicated that the N-terminal region of actin contains one of the binding sites between actin and myosin. Cross-linking experiments have shown that the acidic residues of the actin region (1–12) bound to the 20- and 50-kDa tryptic fragments of myosin subfragment 1, S1 (which contains one globular head of myosin) (Sutoh, 1982, 1983). NMR studies have confirmed that residues in the amino terminus of actin were perturbed during the acto–S1 interaction (Moir & Levine, 1986, Moir et al., 1987). Two independent laboratories produced antibodies specific to sequences within the N-terminal region of actin. Mejéan et al. (1986, 1987) used two antiprotein antibodies with different specificities in the N-terminal region of actin (1–28). The antibody affected by sequence changes at positions 2 and 3 (skeletal vs cardiac actin) only partially inhibited the acto–S1 interaction (determined by ELISA assays). Their second antibody with a suggested epitope favoring the C-terminal region of residues

† This investigation was supported by research grants from the Medical Research Council of Canada and Alberta Heart Foundation and an Alberta Heritage Foundation for Medical Research Studentship (J.V.E.).

0006-2960/91/0430-11676$02.50/0